Modeling and Simulation of Polymeric Nanocapsule Formation by Emulsion Diffusion Method

M. Hassou, F. Couenne, Y. le Gorrec, and M. Tayakout
Laboratoire d'Automatique et de Génie des Procédés, University of Lyon, University Lyon 1, France

DOI 10.1002/aic.11809
Published online June 22, 2009 in Wiley InterScience (www.interscience.wiley.com).

The objective of this work is to develop a predictive dynamical model of a nanoencapsulation process using an emulsion diffusion method. This model describes the formation of the polymeric membrane around the oil droplet and its size reduction due to the solvent diffusion. To this end, we assume that the phase separation is only due to purely diffusive mechanism. This work is illustrated on the formation of poly-ε-caprolactone (PCL) around the oily core formed of labrafac from the initial homogeneous polymer-solvent-nonsolvent solution (PCL, ethyl acetate, and labrafac). The polymeric membrane formation, the size reduction of the nanocapsule after the solvent diffusion, and the morphology of nanocapsules are experimentally investigated. It is shown that the results obtained in simulation from the dynamical model are in agreement with the experimental ones. The model is then used to predict the effect of the initial composition on the nanocapsule morphology. © 2009 American Institute of Chemical Engineers *AIChE J,* 55: 2094–2105, 2009
Keywords: nanocapsule, multicomponent diffusion, phase separation, polymer, modeling

Introduction

Nanoencapsulation of solid or liquid by polymer coating technique[1–7] is widely used in the pharmaceutical field.[8–15] The main benefits of this technique are to improve the stability of the drug, to protect the drug from environmental conditions, and to better control the drug release.

One of the several methods to produce nanocapsules is the emulsion diffusion method. In this process, the formation of nanocapsule is characterized by the diffusion of solvent from an initially homogeneous polymer-solvent-nonsolvent solution. Such diffusion leads to the formation of a turbid two-phase solution. Solidification then follows in which the polymer from the polymer-rich phase precipitates to form a solid membrane which envelops the polymer-lean phase.

Most of the work developed in this field focuses on the experimental studies,[16–19] which are usually time consuming and require extensive trials. This difficulty can be greatly overwhelmed by accurate and reliable mathematical models. Moreover, these models provide a better understanding of effective control of the nanocapsules membrane formation. Indeed, the modeling of kinetics of nanocapsule formation is of great interest because some of their important stages are very fast and may be hardly accessible to a direct experimental observation.

The goal of this work is to provide a model of the mechanisms of the nanocapsule formation and of the polymeric membrane formation.

To represent these mechanisms, phase separation and mass transfer phenomena have to be coupled.

The phase separation of a mixture has been introduced by Gibbs free energy. The phase separation occurs if the system can lower its free energy, i.e., it appears for nonstrictly convex Gibbs free energy function.

The Gibbs free energy of nonideal mixture have two spinodal points corresponding to unstable region limit in which the separation phase occurs.[20] The region between the bimodal and spinodal points is only metastable and corresponds to nucleation mechanism.

Correspondence concerning this article should be addressed to F. Couenne at couenne@lagep.univ-lyon1.fr

In the case of nonideal solvent/polymer mixture, the nonideality of the free energy is represented by the enthalpic part of the Flory-Huggins thermodynamic model.[21] The diffusion in nonideal mixture described by this thermodynamic model fails to be represented by Fickian diffusion as shown by Nauman.[20] This author proposes a solution only for closed system by introducing Cahn-Hilliard formalism (also called spinodal decomposition).

In this article, the system under consideration is open. Consequently, Cahn-Hilliard formalism cannot be applied. So, Fickian diffusion is used with Flory-Huggins model without the enthalpic contribution. The phase separation is approached by using varying diffusion coefficient with respect to polymer concentration.

In the first section, we present the experimental work that we performed to get data related to the mechanism of the nanocapsule formation. This work points out the two phenomena: the membrane formation around the internal phase and the nanocapsule radius reduction.

Afterward, we propose a predictive model of the formation of a single droplet. This model is based on the multicomponent mass transfer and ternary diffusion (with dependency of the diffusion coefficient on the polymer concentration). This model allows both the prediction of spherical polymeric membrane formation as well as the size of this latter following the dilution of the continue phase.

Finally, we present some results obtained from the simulation of the aforementioned model illustrating the internal composition during the solvent diffusion. We study the robustness of this model and discuss about its properties and limitations.

Materials and Methods of Preparation of Nanocapsules

Materials

The polymer used for the nanocapsules formation is poly-ε-caprolactone (PCL; Sigma Aldrich Chemical Company, USA). The core of the nanocapsule is made of an oil, labrafac lipophilic WL 1349, a mixture of triglycerides of fatty acids caprylic (C8)/capric (C10) from Gattefossé. The solvent is the pure ethyl acetate from Laurylab. The stabilizer is polyvinyl alcohol (PVA; Mowiols 40-88, 88% hydrolyzed). Distilled water saturated with solvent is used as a nonsolvent and distilled water as a diluent for the emulsion.

Emulsification–diffusion method

The origin of this technique is due to Quintanar-Guerrero.[22] The nanocapsules are prepared using the emulsification–diffusion process. It is a two-step method, based on the production of an emulsion (Step 1), followed by a dilution with distilled water leading to the deposition of the polymer around the droplets (Step 2), and as a result, the formation of nanocapsules.

The emulsification involves an organic phase and an aqueous phase. The organic phase is composed of partially water-soluble ethyl acetate, previously saturated with water, containing the dissolved PCL and labrafac. The aqueous phase contains the distilled water previously saturated with ethyl acetate and containing PVA. The emulsion is obtained by mixing these two phases.

The polymer emulsion resulting from such treatment is very stable and contains very small droplets (below 0.3 μm diameter). The subsequent addition of a large volume of water to the system causes the solvent diffusion into the external phase, leading to the polymer deposition around the droplets, and the formation of nanocapsules. The solvent is eliminated from the final mixture by evaporation under reduced pressure.

It appears that the formation of nanocapsules occurs during the diffusion step when the organic solvent diffuses out of the organic phase leading to the nascent polymeric membrane. Consequently, our study will be driven by the hypothesis that the mechanism of the nanocapsule formation by emulsion diffusion method is due to diffusion alone.

Preparation of PCL nanocapsules

First, the two mutually saturated phases are prepared. The saturated water contains 8–10% of ethyl acetate and the saturated solvent contains 2–3% of water. The stabilizer PVA is dissolved at a concentration of 2.5% w/w in saturated water at 50°C for 20 min. The labrafac (0.5 g) and the PCL (0.2 g) were dissolved in 20 ml of saturated ethyl acetate at 50°C for 20 min. The resultant organic solution (20 ml) is dispersed into saturated water (40 ml) containing stabilizer using rotor-stator device (Ultraturraxss T25) at 8000 rpm during 5 min in a cylindrical vessel.

The emulsion is formed at 20°C. The dispersed droplets are converted into nanocapsules by the addition of a large volume of water (200 ml) to induce the solvent diffusion. After addition of water in the emulsion and the mixing at 300 rpm, the nanocapsules are formed. Extraction of the solvent and water from the nanocaspsules suspension is achieved by evaporation at 40°C in a rotary evaporator under reduced pressure (50 mbar).

PCL nanocapsules characterization

Particle Size Evolution. The size of the nanocapsule is a very important parameter because it is one of the factors to control the kinetics of drug release. Consequently, it is important to characterize this parameter. Unfortunately, the investigation of the dynamics of particle size evolution gives rise to many experimental difficulties. The main experimental difficulties are due to the fast rate of diffusion of the solvent and from the small size of the particles that do not allow continuous measurements.

To overcome these difficulties, we assume that the system goes through an infinity of thermodynamic equilibrium states and that each equilibrium state corresponds to the amount of water present in the external phase. At the end of this process, we assume that nanocapsules are similar in size and composition as those obtained by the standard method. So we propose to add regularly a small amount of distilled water and then to measure the mean diameter of nanocapsules. Accordingly, a partial diffusion of the solvent out of the emulsion droplets is performed by means of these discontinuous dilutions. This technique slows down the diffusion process and consequently

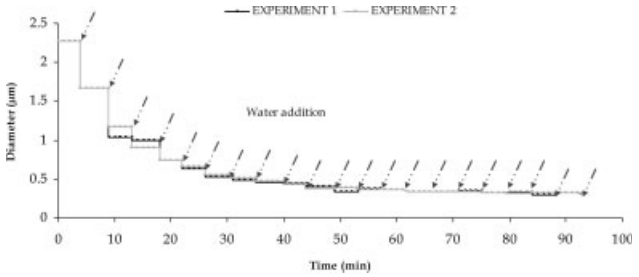

Figure 1. The evolution of the nanocapsule diameter for two same experiments.

it enables to explore the different intermediate states taking place during the dilution step.

We consider an emulsion oil–water prepared accordingly to the previous operational protocol.

The mean particle size of the nanoparticles is assessed by the Nanotrac from Granuloshop (NAS35 Autosampler) while plunging the probe of the Nanotrac in the sample. This technique uses an advanced power spectrum analysis of Doppler shifts to produce a full volume distribution of particle sizes. Any additional dilution of the suspension is not required for this technique.

The operating procedure for the assessment with Nanotrac is the following: After each dilution with 10 ml of distilled water, 1 min is necessary for stirring the suspension. Then the suspension is released after 1 min as the assessment is based on Brownian motion. One additional minute is necessary for the measurement.

The evolution of the size of the nanocapsules according to time and to the quantity of water added in the external phase is investigated. Figure 1 presents the evolution of the size of the nanocapsules for two similar experiments.

The arrows in Figure 1 correspond to the addition of 10 ml of water. These experiments show that the diameter of the nanocapsule decreases continuously with the increase of the quantity of water and that the experiments are repeatable.

Assuming that there is no solvent evaporation, the comparison of the emulsion (diameter at $t = 0$) and of nanocapsule suspension size distributions (diameter at $t = t_{final}$) shows that the solvent diffusion occurs only after the emulsion formation, while the dilution water is added. This diffusion results in the transformation of each droplet in a particle of smaller size.

These observations show that the formation of nanocapsule by emulsion–diffusion is a dynamic process that can be associated with the diffusion of the solvent from the droplet to the external phase.

Internal Morphology Study. Few data on structural organization of the nanocapsules constituents are available in literature. The presence of an oil ''capsular'' structure surrounded by a polymeric envelope is only suggested by hypotheses. However, the structure of the particle and the thickness of the membrane are very important parameters because they play a major role in the protection of the drug and in the kinetics of drug release.

To obtain information about the formation and morphological characteristics of nanocapsules, the transmission electronic microscopy (TEM) is used after cryofracture before and after complete dilution as shown in Figure 2.

In this experiment, the emulsion is quickly frozen in liquid nitrogen (−210°C), which clamps down the emulsion components instantly.

The illustrations of the Figure 2 show the internal organization and the structure of the nanocapsule within the emulsion.

The TEM observation, before dilution (Figure 2a), shows a homogenous structure inside the nanocapsule with no contrast. In Figure 2b, the particle core has a different contrast from that of the shell; it has a capsular structure with homogeneous shell. Moreover, the surface of the nanocapsule becomes smoother after solvent diffusion.

In both cases, well-defined particles having spherical form can be observed. The diameters measured on the pictures are in good agreement with those determined by light scattering analysis.[23] It also confirms, as seen with the first experiment, the reduction of the radius of the nanocapsule. The mean value thickness of the membrane thickness is estimated to be about 15 nm from direct manual measurements on the pictures.

Modeling of Nanocapsule Formation

To model the formation of the nanocapsules by emulsion diffusion process, we investigate the problem of a single droplet. This droplet is suddenly plunged into an infinite aqueous phase. We also assume that outside the droplet, the

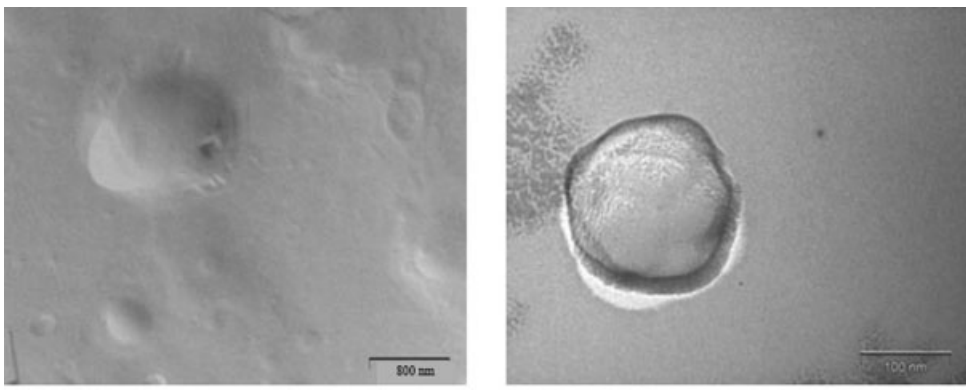

Figure 2. Internal structure of the nanocapsule before (a; at $t = 0$) and after dilution (b; at $t = t_{total}$).

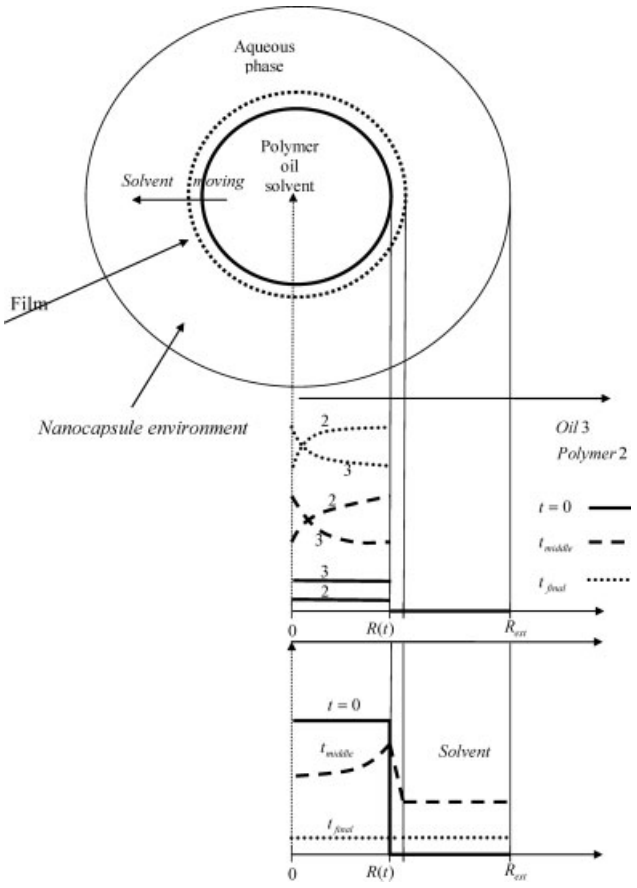

Figure 3. Schematic description of nanocapsule formation and time evolution of mass fraction of species.

solvent concentration is kept equal to zero because of both perfect stirring and infinite dilution. We represent this system as two concentric spheres as shown in Figure 3. The large sphere represents the aqueous phase and the small one represents the droplet.

We make the following assumptions:

- There are two systems, the external one which represents the exterior of the nanocapsule {solvent + nonsolvent} and the internal one {solvent–water + polymer + oil}. The stabilizer is not taken into account. We assume that it does not participate to mass transfer phenomena. It stays around the nanocapsule to stabilize it.
- Only three components are inside the nanocapsule (solvent, polymer, oil). The solvent is saturated with water but has the same behavior of that of the solvent alone.
- Nanocapsules are represented by symmetrical spheres with average radius $R(t)$.
- Diffusion inside the droplet is described by Stefan-Maxwell according to the radial coordinate r is considered.
- The mass transfer outside the droplet is proportional to the droplet dissolution rate.
- The molar volume of the polymer is constant.
- The mass transfer at the interface of the droplet is described by a film model.

We assume that the nanocapsule polymeric membrane formation is due to purely diffusive processes, which causes the polymer accumulation. When the polymer accumulation exceeds some solidification concentration, the solidification of the accumulated polymer takes place and the polymeric membrane is formed.

It leads to the following assumption:

- We assume that both diffusion coefficients of polymer–solvent and polymer–nonsolvent are function of the polymer volume fraction. These diffusion coefficients are represented by empirical functions that we establish.

The empirical laws are chosen such that the diffusion coefficient decreases. The empirical laws are chosen such that the diffusion coefficient decreases from its initial value to the solidification concentration for which the polymer does not diffuse anymore.

Moreover, the Maxwell-Stefan model expresses the chemical potential as a function of the flux variables. Consequently, to compute these flux variables, it is necessary to inverse this function leading to the constraint that the diffusion coefficients never equals to zero during the simulation. So the empirical functions are chosen such that the diffusion coefficient tends to a small value when the polymer volume fraction tends to the critical value.

Model Formulation. First, we present the constitutive relations used for modeling the mass transfer as well as the thermodynamic phenomena. Then, the different mass balances and the differential equation driving the evolution of the radius of the nanocapsules are given. Finally, boundary conditions are presented.

Mass transfer model. In several works, the Maxwell-Stefan approach has been adopted to model the multicomponent mass transfer.[24] The driving forces are given as a linear combination of the material fluxes.

Maxwell-Stefan model has been successfully applied to describe multicomponent diffusion in simple fluid mixtures.[24] Recently, it has also been used to describe transport through polymeric membranes in a solution–diffusion framework. However, application of Maxwell-Stefan model to a solvent–membrane system presents a problem: the molar concentration of the membrane is ill defined as its molecular weight is unknown.[25]

To circumvent this deficiency, several suggestions have been proposed in the literature.[26–31] Nevertheless, the Extended Maxwell-Stefan theory (EMS) developed by Fornasiero et al.[32] remains the most attractive one. This model is developed for solutions of molecules that have starkly different sizes.

In the EMS theory, the polymer molecule is modeled as a collection of segments connected together. Each segment has roughly the size of the solvent molecule, and all segments in the polymer molecule have identical frictional properties. When compared with the classical Maxwell-Stefan model, in the EMS formalism, the friction factor k_{ij} between the colliding molecules i and j is related to the molar segment concentrations instead of the molar species concentrations. Its expression is given in Eq. 1:

$$k_{ij} = RT \frac{c_i^0 c_j^0}{c_T^0 \mathcal{D}_{ij}^0} \tag{1}$$

where the superscript 0 refers to segments.

According to EMS theory, diffusive fluxes are related to the driving forces (gradients of the chemical potentials) by Eq. 2:

$$-c_i\nabla_{T,P}\mu_i = RT\sum_{\substack{j=1\\ j\neq i}}^{N_c}\frac{c_i^0 c_j^0}{c_T^0 \mathcal{D}_{ij}^0}\left(\frac{N_i^0}{c_i^0}-\frac{N_j^0}{c_j^0}\right),\quad i=1,2,...,N_c \tag{2}$$

where $\nabla_{T,P}\mu_i$ is the gradient of chemical potential for species i and N_i^0, N_j^0 are the molar flux of segments of species i and j, respectively.

Fornasiero et al.[32] assume that there is no volume change upon mixing and convert the segment mole fraction into a species volume fraction ϕ_i^0 according to Eq. 3:

$$c_i^0 = \frac{\phi_i^0}{v^0} \tag{3}$$

with $\phi_i^0 = \phi_i$ and $c_i^0 = c_i n_s^i$.

Although the choice of the segment unit (and therefore the choice of the molar volume v_i^0) is arbitrary, it is reasonable, based on physical arguments,[32] to assume that the sizes of all segments and for all species i are the same. From this assumption, for any species i, we have $v^0 = v$, and the total segment concentration is $c_T^0 = 1/v$. A convenient choice for v is the molar volume of the pure solvent or the molar volume of the component that has the smallest molecules. This choice of v is identical to the lattice size in Flory-Huggins polymer solution theory,[33] which is widely used to express the chemical potential of a species in a polymer solution or in a membrane as a function of the condensed-phase composition.[33]

Then Eq. 2 becomes

$$-c_i\nabla_{T,P}\mu_i = RT\sum_{\substack{j=1\\ j\neq i}}^{N_c}\frac{1}{\mathcal{D}_{ij}^0}(\phi_i N_j^0 - \phi_j N_i^0), i=1,2,...,N_c \tag{4}$$

Finally, let us notice that EMS theory is consistent with restrictions given by the Gibbs-Duhem equation and by Onsager's reciprocity relations. By the Gibbs-Duhem relationship given in Eq. 5, only ($N_c - 1$) chemical potential gradients are independent.

$$\sum_{i=1}^{N_c} n_i\Delta\mu_i = \sum_{i=1}^{N_c}\frac{\phi_i}{n_s^i v^0}\Delta\mu_i = 0 \tag{5}$$

To emphasize the influence of species on the molar fluxes of segments, let us write the expression of segment flux of each component as it will appear in the model. For this purpose, we have to take into account the constraints on volume fractions and molar fluxes:

$$\begin{cases}\sum_{i=1}^{N_c}\phi_i = 1\\ \sum_{i=1}^{N_c} N_i^0 = 0\end{cases} \tag{6}$$

We then obtain the relations:

$$\begin{pmatrix}-c_1\nabla_{T,P}\mu_1\\ -c_2\nabla_{T,P}\mu_2\end{pmatrix} = RT\begin{bmatrix}\frac{-\phi_2}{\mathcal{D}_{12}^0}-\frac{(1-\phi_2)}{\mathcal{D}_{13}^0} & \frac{\phi_1}{\mathcal{D}_{12}^0}-\frac{\phi_1}{\mathcal{D}_{13}^0}\\ \frac{\phi_2}{\mathcal{D}_{21}^0}-\frac{\phi_2}{\mathcal{D}_{23}^0} & \frac{-\phi_1}{\mathcal{D}_{21}^0}-\frac{(1-\phi_1)}{\mathcal{D}_{23}^0}\end{bmatrix}\begin{pmatrix}N_1^0\\ N_2^0\end{pmatrix} \tag{7}$$

Mass balance inside the nanocapsule. The continuity equation for component i in the nanocapsule is obtained from the differential material balance. Considering the segment volume fraction, one can write

$$\frac{\partial\phi_i(t,r)}{\partial t} = -\frac{v^0}{r^2}\frac{\partial(r^2 N_i^0)}{\partial r} \tag{8}$$

where the diffusion flux of segments of component i, N_i^0, is defined by Eq. 4.

Mass balance outside the nanocapsule (external phase). For the sake of clarity, the component system solvent (ethyl acetate), polymer (PCL), and oil (triglyceride mixture) are denoted as 1, 2, and 3, respectively.

The rate of change of the solvent mole number n_1^{ext} is given by:

$$\frac{dn_1^{ext}}{dt} = V_{ext}\frac{dc_1^{ext}}{dt} + c_1^{ext}\frac{dV_{ext}}{dt} \tag{9}$$

where V_{ext} is the volume of the external phase which is defined as follows:

$$V_{ext} = \frac{4\pi}{3}(R_{ext}^3 - R_t^3) \tag{10}$$

Outside the nanocapsule, only the solvent diffuses. Consequently, the fluxes of the other components are equal to zero. Moreover, the mass transfer at the interface of the sphere is described by the film model: it is assumed that all of the resistance to the mass transfer is concentrated in a thin film, or layer, adjacent to the boundary.[24] So the rate of change of the number of mole of solvent is

$$\frac{dn_1^{ext}}{dt} = \overbrace{K_1^e\left(c_1^* - c_1^{ext}\right)}^{N_1} S = \frac{K_1^e}{n_s^1}(\phi_1^* - \phi_1^{ext}) \tag{11}$$

Replacing $\frac{dV_{ext}}{dt}$ and V_{ext} by their values in Eqs. 9 and 10 and rearranging Eq. 11 by Eq. 10, we finally obtain the rate of change of the solvent concentration in the external phase:

$$\frac{d\phi_1^{ext}}{dt} - \frac{3\phi_1^{ext}R_t^2}{(R_{ext}^3 - R_t^3)}\left(\frac{dR_t}{dt} - K_1\right) - \frac{3K_1\phi_1^* R_t^2}{(R_{ext}^3 - R_t^3)} = 0 \tag{12}$$

The rate change of the nanocapsule radius. The objective of this paragraph is to point out the correlation between the nanocapsule radius motion and the mass transfer rate at the interface. Because of the solvent diffusion toward the external phase, the nanocapsule radius R_t moves with the velocity $\frac{dR_t}{dt}$. Only the solvent diffuses at the interface of the nanocapsule. Therefore, the rate change of the total mole

number corresponds to the solvent quantity which diffuses toward the external phase. So it is given by Eq. 13:

$$\frac{dn_t}{dt} = N_{t(r=R_t)} S \tag{13}$$

We assume that the molar fluxes of polymer and of oil at the interface of the nanocapsule are equal to zero: $N_{2(r=R_t)} = N_{3(r=R_t)} = 0$. So the total flux is given by $N_{t(r=R_t)} = N_{1(r=R_t)}$. We finally deduce the following:

$$\frac{dn_t}{dt} = -\frac{dn_1^{\text{ext}}}{dt} \tag{14}$$

The total mole number is calculated as follows:

$$n_t = \frac{V_t}{v^0} \sum_{i=1}^{N_c} \frac{\overline{\phi_i}|_{V_t}}{n_s^i} \tag{15}$$

where $\overline{\phi_i} = \frac{4\pi}{V_t} \int_0^R \phi_i r^2 dr$ is the mean value of the volume fraction in the nanocapsule.

Using this relation, the derivative of n_t is given by:

$$\frac{dn_t}{dt} = \frac{4\pi R_t^3}{3v^0} \sum_{i=1}^{N_c} \frac{1}{n_s^i} \frac{d\overline{\phi_i}|_{V_t}}{dt} + \frac{4\pi R(t)^2}{v^0} \frac{dR_t}{dt} \sum_{i=1}^{N_c} \frac{\overline{\phi_i}|_{V_t}}{n_s^i} \tag{16}$$

By Eq. 11, the rate change of the nanocapsule radius meets the relation

$$\frac{R_t}{3} \sum_{i=1}^{N_c} \frac{1}{n_s^i} \frac{d\overline{\phi_i}|_{V_t}}{dt} + \frac{dR_t}{dt} \sum_{i=1}^{N_c} \frac{\overline{\phi_i}|_{V_t}}{n_s^i} + \frac{K_1}{n_s^1} (\phi_1^* - \phi_1^{\text{ext}}) = 0 \tag{17}$$

where the equilibrium volume fraction of solvent ϕ_1^* is given by

$$\phi_1^* = k_1^e \phi_1|_{R_t} \tag{18}$$

Boundary conditions

The calculation of the boundary conditions is done in accordance with classical methods already presented in literature.[34,35] This model is solved in taking into account the following boundary conditions

$$\text{At } r = 0 \qquad N_i^0 = 0 \quad i = 1, 2, 3 \tag{19}$$

At the interface, the continuity of flux is set down. So the continuity of flux of species 1, 2, and 3 at the moving boundary R_t has to be computed. As previously mentioned, the molar flux of polymer and oil at the interface of the nanocapsule is equal to zero. So, the molar flux of solvent is not equal to zero.

Using the Leibniz integral rule, the time variation of the volume fraction over the moving volume of component i is computed:

$$\frac{d}{dt} \int_0^{R_t} 4\pi \phi_i(t,r) r^2 dr = \int_0^{R_t} \frac{\partial \phi_i(t,r)}{\partial t} 4\pi r^2 dr + 4\pi R_t^2 \phi_i(t, R_t) \frac{dR_t}{dt} \tag{20}$$

Considering mean values, the left term of equality 20 leads to the following mole balance:

$$\frac{1}{n_s^i v^0} \frac{d(\overline{\phi_i} V_t)}{dt} = \frac{dn_i}{dt} \tag{21}$$

Using Eq. 8, the first term of the right member of the equality 20 can be replaced. So Eq. 20 becomes

$$n_s^i v^0 \frac{dn_i}{dt} = \int_0^{R_t} -\frac{v^0}{r^2} \frac{\partial (r^2 N_i^0)}{\partial r} 4\pi r^2 dr + 4\pi R_t^2 \phi_i(t, R_t) \frac{dR_t}{dt} \tag{22}$$

Finally, we obtain the following relation for flux at the moving boundary:

$$n_s^i v^0 \frac{dn_i}{dt} = 4\pi v^0 R_t^2 N_i^0(R_t) + 4\pi R_t^2 \phi_i(t, R_t) \frac{dR_t}{dt} \tag{23}$$

It is due to the following boundary conditions:

$$\text{At } r = R_t \quad \begin{cases} \dfrac{N_1^0|_{R_t}}{n_s^1} - \dfrac{dR_t}{dt} \dfrac{\phi_1|_{R_t}}{n_s^1 v^0} = K_1 (c_1^* - c_1^{\text{ext}}) \\ \dfrac{N_1^0|_{R_t}}{n_s^i} - \dfrac{dR_t}{dt} \dfrac{\phi_i|_{R_t}}{n_s^i v^0} = 0 \quad i = 2, 3 \end{cases} \tag{24}$$

with $c_1^* = \dfrac{\phi_1^*}{n_s^1 v^0}$.

Numerical resolution

These equations are spatially discretized using the finite volume method with a variable grid size; one hundred finite volumes are used. It leads to a system of differential algebraic equations. This resulting model is strongly nonlinear and stiff. It is solved using the Petzold-Gear method (DDASPG routine of the IMSL package).

Simulation. According to the model developed, a numerical algorithm has been developed using the FORTRAN language.

Table 1. Physical Parameters

	Solvent Ethyl Acetate	Oil Labrafac	Water	Polymer PCL
Molar mass (g/mol)	88.12	470	18	80,000
Density (mass volume/mass volume of water)	0.902	0.946	1	1.145
Viscosity (mPa s)	0.44	26	1	–
Molar volume ($\times 10^{-6}$ m^3/mol)	97.69	456.83	18	12,459
Temperature (K)	293	293	293	293

Table 2. Mass Transfer Coefficients

	Acetate/Water	Acetate/Labrafac	Labrafac/Acetate
$\mathcal{D}_{ij}^{\circ}$ (m^2/s)	–	9.31×10^{-8}	1.85×10^{-8}
K_1 (m/s)	4.43×10^{-5}	–	–
k_i^e (–)	0.092		

Table 3. Initial States for the Model

Model Input	Value
Solvent volume fraction (–), $\phi_1^e(t=0,r)$	0.996
Polymer volume fraction (–), $\phi_2^e(t=0,r)$	0.001
Radius of the capsule (m) R_t $(t=0)$	1.135×10^{-6}

Results and Discussion

Model parameters

All physical parameters are given in Table 1.

Mass transfer parameters

The Mass Transfer Coefficient for the Solvent. The mass transfer coefficient K_1 (m/s) is the ratio between the coefficient of diffusion in the film and the film thickness. It is calculated using the correlation of Wakao and Funazkri[36]:

$$Sh = 2.0 + 1.1Sc^{1/3}\,Re^{0.6}$$

The Diffusion Coefficients of Liquids. The diffusion coefficients of the oil in the solvent are defined using the Vignes[37] equation: $\mathcal{D}_{ij} = (\mathcal{D}_{ij}^{\circ})^{x_i}(\mathcal{D}_{ji}^{\circ})^{x_j}$. $\mathcal{D}_{ij}^{\circ}$ is the infinite dilution coefficient of species i in species j. It is estimated using the Wilke-Chang[38] equation:

$$\mathcal{D}_{ij}^{\circ} = 7.4 \times 10^{-8}\,\frac{(\Theta_j M_j)^{1/2} T}{\eta_j^v v_m^i}$$

Results are summarized in Table 2.

The Diffusion Coefficients of Liquids in the Polymer. To represent the polymeric membrane apparition, we assume that the membrane formation is attributed to the direct accumulation–solidification of the polymer. The solvent diffusion induces the polymer accumulation and subsequent formation of the polymeric membrane. Consequently, one can assume that the polymer diffusion coefficients depend on its volume fraction.

As described in the assumptions of modeling paragraph, we assume that the diffusion coefficients are decreasing exponentially with the polymer volume fraction ϕ_2. The empirical laws are chosen as decreasing functions. They fulfill some consistent order of magnitude when ϕ_2 tends to be 0 or the solidification volume fraction:

- Diffusion coefficients of the polymer in the solvent (m^2/s): $\mathcal{D}_{21} = 10^{-8}(10^{-100\phi_2}) + 10^{-19}$
- Diffusion coefficients of the polymer in the nonsolvent (m^2/s): $\mathcal{D}_{23} = 10^{-10}(10^{-60\phi_2}) + 10^{-19}$

Figure 4 gives the shape of these diffusion coefficients with respect to ϕ_2 and shows that the solidification volume fraction is about $\phi_2 = 0.015$. The decrease rate of the diffusion coefficient of the polymer in the solvent is chosen bigger than the one of the diffusion coefficient of the polymer in the nonsolvent. When the polymer solvent fraction increases, these coefficients decrease and tend toward zero, the molar flux becomes negligible. The phase separation gives rise to a solid polymer that does not diffuse.

Finally, the initial states are given in Table 3.

To compare the experimental results with the simulation, the input solvent volume fraction $\phi_1^{\text{ext},e}(t,r)$ is represented by a succession of steps as shown in Figure 5.

Simulation results: Comparison with the experiment

The simulation results corresponding to previously given initial states and inputs are shown in Figure 6.

In the simulation using the same initial composition as for experiment, the nanocapsule diameter decreases until about 419 nm at the end of experiment. This value is very similar to the experimental data which shows a final reduction of the nanocapsule diameter to 320 nm. In general, a good agreement is obtained between the simulation results and experimental data. It strengthens the hypothesis of the nanocapsule size reduction associated with a solvent diffusion.

To figure out the phase separation induced via the diffusion coefficients of polymer/solvent and polymer/nonsolvent,

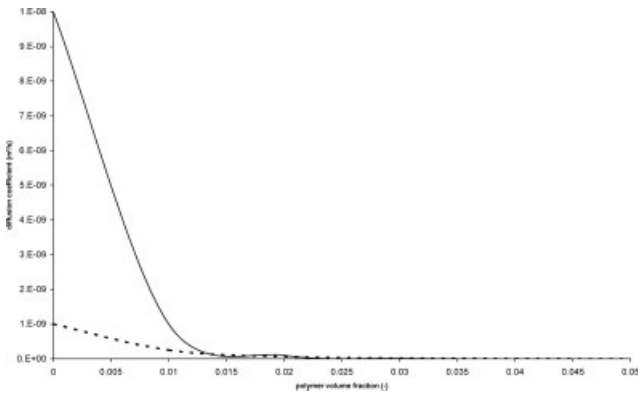

Figure 4. Diffusion coefficients $\mathcal{D}_{21}$ (–) and $\mathcal{D}_{23}$ (--) vs. ϕ_2.

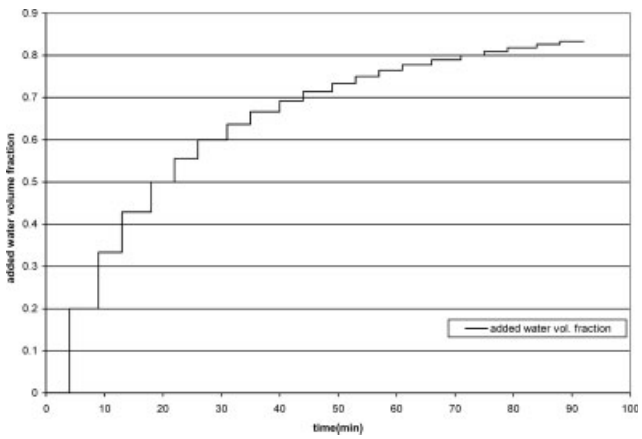

Figure 5. Added solvent volume fraction with respect to time.

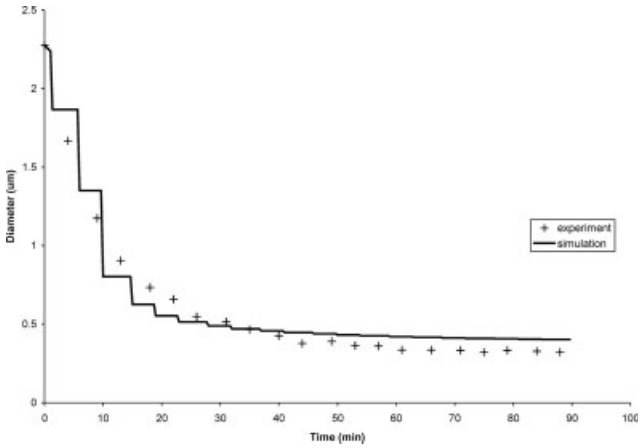

Figure 6. Nanocapsule diameter prediction (μm) and experimental data.

the process is simulated in real conditions where the total quantity of water (200 ml) is added at one time. The calculated solvent fraction input $\phi_1^{\text{ext},e}(t = 0, r)$ is then equal to 0.0152. The polymer volume fraction at several radial positions (100 volumes are chosen for spatial discretization) and the diameter evolutions are represented in Figures 7 and 8, respectively.

As shown in Figure 7, the polymer volume fraction reaches its maximum at the interface of the nanocapsule. This interface corresponds to the 8% of the radius. This result reproduces the polymeric membrane formation observed from the experiment. The thickness of the membrane is approximately equal to 17 nm—close to the experimentally measured thickness 15 nm as already given in previous section.

Moreover two zones can be pointed out:

- The first zone from $t = 0$ h to $t = 3$ h with small enrichment at the interface.
- The second zone from $t = 3$ h with the phase separation induced by the polymer diffusion coefficients through their dependency on polymer volume fraction. It can be observed that there are two phases: the first one is rich in oil and is located in the center, and the second one is rich in polymer and is located at the interface of the nanocapsule.

This phenomenon represents the solidification of the polymer. Consequently, the polymer remains at the nanocapsule interface and forms a porous membrane around the oil.

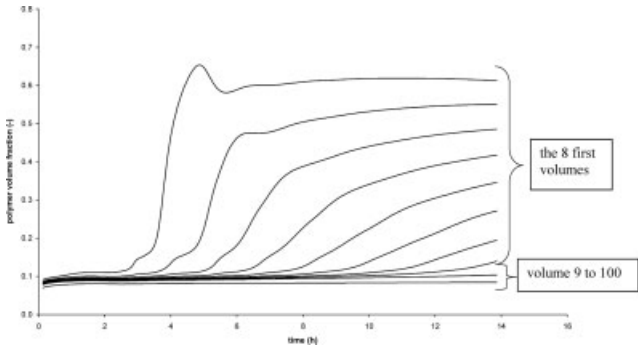

Figure 7. Polymer volume fraction evolution vs. time.

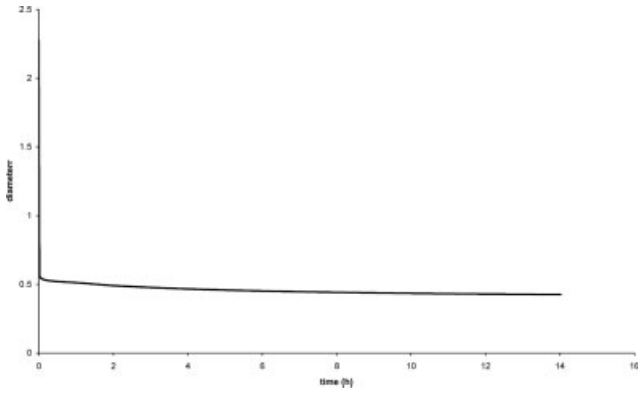

Figure 8. Diameter evolution (μm) vs. time.

Figure 8 shows that the 419-nm final diameter is reached at time 14 h. The diameter decreases rapidly to 500 nm in 2 min and then this decrease is slowed down.

Figures 7 and 8 show two distinct dynamics: the faster one corresponding to the solvent extraction and the slower one to the reorganization in the nanoparticle. The membrane formation occurs after the extraction of the majority of solvent.

Remarks. At infinite time, this model does not represent the final state of nanocapsule. It does not take into account the complete solidification of the polymer. Indeed, at the end of the nanocapsule formation, the polymer–solvent and polymer–nonsolvent diffusion coefficients decrease to 10^{-18} and remains at this value. As a consequence, the system will return to the new thermodynamical equilibrium after a long time, which is not represented in Figure 7.

Simulation results: Influence of the polymer/oil initial volume ratio

The increase of polymer concentration. Simulations are performed for two polymer/oil initial ratios (1/6, 5/6) and are compared with the previous one (1.5/6). The effects on the diameter evolution and polymer volume fraction evolution are represented in Figures 9–11.

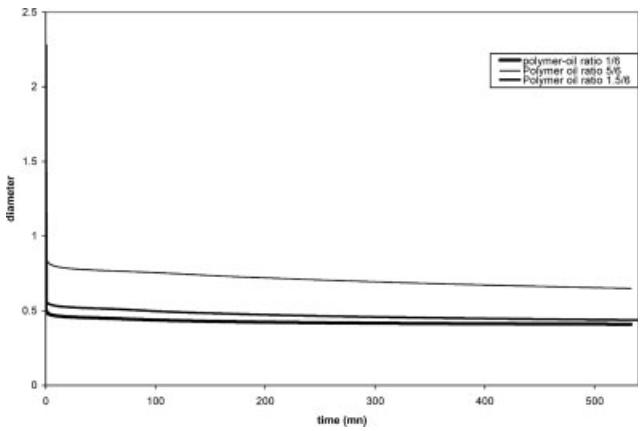

Figure 9. Diameter (μm) vs. time (min) for different polymer oil mass ratio and constant volume fraction of solvent.

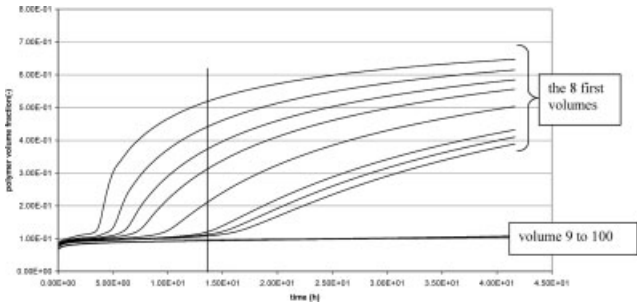

Figure 10. Polymer volume fraction vs. time for polymer oil 5/6 mass ratio and constant volume fraction of solvent.

Figure 9 shows that the diameter increases with the increase of the polymer/oil ratio. The increase of the polymer/oil ratio is equivalent to the increase of the concentration of polymer. This simulation result is in agreement with the experimental results presented in Guinebretière et al.[19,39]

Figures 10 and 11 give the polymer volume fraction evolutions.

The vertical bar situated at $t = 14$ h permits to compare more easily the evolution of the polymer volume fractions with the one given in Figure 7. They show that the transitory dynamic decreases with respect to the increase of the initial polymer/oil ratio. Moreover, the thickness of the nanocapsule increases with respect to the increase of the initial polymer/oil ratio, as also mentioned by Loxley et al.[40] The thicknesses are 16.4, 17.4, and 26.4 nm for initial ratios 1/6, 1.5/6, and 5/6, respectively.

Finally, comparing the structure of the polymer membrane at time $t = 14$ h, we can observe the following:

- This membrane is richer in polymer when the initial polymer/oil ratio increases. In Figure 11 it can be observed that the enrichment of the membrane is about $\phi_2 = 0.17$ for the first 8 volumes and $\phi_2 = 0.1$ for the other 92. So it can be concluded that for very small polymer/oil ratio, the structure tends to a nanosphere[40] where the polymer is homogeneously distributed in the capsule.
- The dynamic of polymer enrichment of the membrane decreases when the initial polymer/oil ratio increases. In Figure 10, the polymer enrichment of the membrane has not reached its maximum at time $t = 14$ h. The structure tends to a nanocapsule[40] where the polymer is concentrated at the interface.

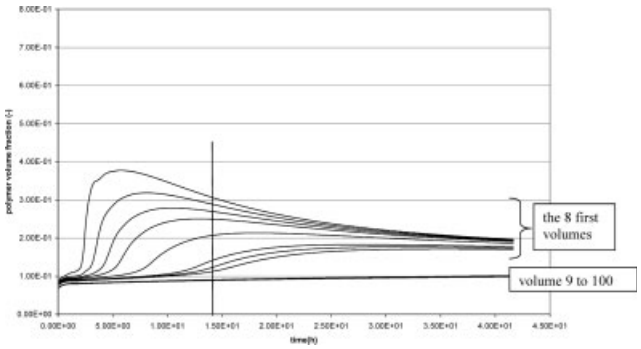

Figure 11. Polymer volume fraction vs. time for polymer oil 1/6 mass ratio and constant volume fraction of solvent.

Table 4. Experimental and Simulated Membrane Mean Size and Membrane Thickness for Different Oil Concentration

Polymer/Oil Ratio	Experimental Mean Size (nm)	Simulated Mean Size (nm)	Experimental Membrane Thickness (nm)	Simulated Membrane Thickness (nm)
1/2.5	483 ± 30	414	22 ± 1.5	33
1/2	376 ± 23	402	20.5 ± 1.2	36
1/1	351 ± 20	377	32 ± 1.8	45
1/0.5	360 ± 4	365	50 ± 0.5	51

The increase of oil concentration. To study the effect of the increase of the oil concentration with respect to nanocapsule diameter and membrane thickness, different operating conditions given in Table 1 of Ref. 39 are simulated. For this simulation, the initial polymer volume fraction and the initial radius of the capsule are the same as given in Table 3. The total quantity of water (200 ml) is added at one time. The initial oil volume fraction is computed with respect to the simulated ratio. Simulation results and experimental data[39] are summarized in Table 4.

The simulated and experimental results show the same tendencies. The diameter decreases and the thickness membrane increases with respect to the decrease of oil concentration.

Simulation results: Influence of the acetate initial volume ratio

Finally, Figure 12 shows that the size of nanocapsule is inversely proportional to the volume of solvent. These simulation results are in agreement with experimental results presented by Guinebretière et al.[39]

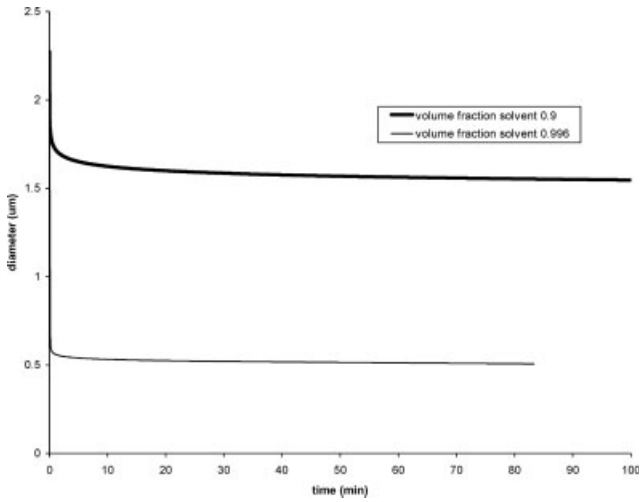

Figure 12. Diameter vs. time for different volume fraction of solvent.

Conclusions

The main purpose of this work is to study the formation of the polymeric membrane during the nanocapsule synthesis using emulsion diffusion process. This polymeric membrane plays a predominant role for the protection of incorporated drugs as well as for the release profile.

A model using polymer concentration varying diffusion coefficients is proposed to capture the nanocapsule formation. This model is able to describe the polymeric membrane formation at the interface of the nanocapsule and the time evolution of the size of the nanocapsule induced by solvent extraction. The diffusion phenomena are described using Maxwell-Stefan equation written in the formalism of Fornasiero,[32] allowing global mass balance conservation for species with starkly different sizes.

To take into account the formation of the polymeric membrane with the constraint that the polymeric membrane flux is never equal to zero, we assume that the polymer diffusion coefficient decreases within a large interval. The polymer diffusion coefficient values are chosen as empirical decreasing function of polymer concentration.

The resulting model is then used to simulate the polymeric membrane formation and to study how the results are influenced by the process inputs.

The results obtained with different initial compositions show that the internal structure of the nanocapsule strongly depends on the polymer/oil ratio. Using this model, we are able to predict the internal structure of the nanoparticles and the polymeric membrane thickness according to input variables (the polymer/oil ratio for example).

Comparison between practical experiments giving the radius evolution and the corresponding simulations have shown a good agreement. The model assumptions are satisfied and the developed model can be used to represent the structure of the nanocapsule.

Notation

c_i^* = equilibrium molar concentration of the component i (mol/m^3)
c_i = molar concentration of the component i (mol/m^3)
c_{ext}^i = external molar concentration of the component i (mol/m^3)
c_i^0 = segment molar concentrations of species i (mol/m^3)
c_T^0 = total segment concentration (mol/m^3)
$\mathcal{D}_{ij}^0$ = EMS diffusivity (cm^2/s)
$\mathcal{D}_{ij}^\infty$ = infinite dilution coefficient of the species i in the species j (cm^2/s)
g = free energy of mixing per unit of volume (j/m^3)
K_i = mass transfer coefficient (mol/s)
k_1^e = equilibrium constant
k_{ij} = friction factor [j/(m^4 s)]
M_j = molar masse of j (g/mol)
N_i = molar flux of the component i [mol/(m^2 s)]
N_i^0 = segment molar flux of the component i [mol/(m^2 s)]
N_c = number of component (–)
n_i = mole number of the component i (mol)
n_i^{ext} = mole number of the component i in the external phase (mol)
n_p = total number of particles (volume of the organic phase/volume of particle)
n_t = total number of moles (mol)
n_s^i = number of segments per molecule of species i (–)
r = radial coordinate (m)
R = ideal gas constant [j/(mol K)]
R_{ext} = radius of a sphere which represents the nanocapsule's environment (m)
R_t = nanocapsule radius (m)
S = total interfacial area for mass transfer (m^2)
v_i^0 = molar volume of segment i (cm^3/mol)
v_i^m = molar volume of the component i (cm^3/mol)
V_{ext} = volume of the external phase (m^3)
V_T = total volume of the emulsion (m^3)
t = time (s)
T = average temperature (K)
x_i = molar fraction for species i (–)

Species

1 = solvent (ethyl acetate)
2 = polymer (PCL)
3 = oil (triglyceride mixture)

Greek letters

χ_{ij} = Flory-Huggins interaction parameter between species i and j (–)
ϕ_i = volume fraction of the species i (–)
ϕ_i^0 = volume fraction of the segments of the species i (–)
ϕ_i^e = initial volume fraction of the species i (–)
ϕ_i^{ext} = volume fraction of the species i outside the nanocapsule (–)
$\phi_i^{\text{ext},e}$ = initial volume fraction of the species i outside the nanocapsule (–)
$\overline{\phi_i|_{V_t}}$ = total volume fraction of the species i in the volume V_t (–)
ϕ_i^* = volume equilibrium fraction of the species i at interface (–)
μ_i = chemical potential of species i (j/mol)
η_j^v = viscosity of j (mPa s)
Θ_j = association factor of the species j (–)

Adimensional number

$Sh \equiv \frac{2K_iR_p}{D_{ij}}$ = number of Sherwood
$Sc \equiv \frac{\mu_i}{\rho_i D_{ij}}$ = number of Schmidt
$Re \equiv \frac{2\rho_i R_p u}{\mu_i}$ = number of Reynolds

Literature Cited

1. Cellesi F, Tirelli N. Sol–gel synthesis at neutral pH in W/O microemulsion: a method for enzyme nanoencapsulation in silica gel nanoparticles. *Colloid Surf A*. 2006;288:52–61.
2. Corradi AB, Bondioli F, Ferrari A, Focher B, Leonelli C. Synthesis of silica nanoparticles in a continuous-flow microwave reactor. *Powder Technol*. 2006;167:45–48.
3. Ruys AJ, Mai YW. The nanoparticle-coating process: a potential sol–gel route to homogeneous nanocomposites. *Mater Sci Eng A*. 1999;265:202.
4. Zhang JX, Gao LQ. Nanocomposite powders from coating with heterogeneous nucleation processing. *Ceram Int*. 2001;27:143.
5. Chang SY, Liu L, Asher SA. Preparation and properties of tailored morphology, monodisperse colloidal silica-cadmium sulfide nanocomposites. *J Am Chem Soc*. 1994;116:6739.
6. Cohen H, Levy RJ, Gao J, Kousaev V, Sosnowski S, Slomkowski S, Golomb G. Sustained delivery and expression of DNA encapsulated in polymeric nanoparticles. *Gene Ther*. 2000;7:1896.
7. Wang Y, Dave RN, Pfeffer R. Polymer coating/encapsulation of nanoparticles using a supercritical anti-solvent process. *J Supercrit Fluids*. 2004;28:85–99.
8. Limayem I, Charcosset C, Fessi H. Purification of nanoparticle suspensions by a concentration/diafiltration process. *Sep Purif Technol*. 2004;38:1–9.
9. Bouchemal K, Briançon S, Fessi H, Chevalier Y, Bonnet I, Perrier E. Simultaneous emulsification and interfacial polycondensation for the preparation of colloidal suspensions of nanocapsules. *Mater Sci Eng C*. 2006;26:472–480.

10. Bhardwaj V, Hariharan S, Bala I, Lamprecht A, Kumar N, Panchagnula R, Kumar MNVR. Pharmaceutical aspects of polymeric nanoparticles for oral delivery. *J Biomed Nanotechnol*. 2005;1:235–258.
11. Kreuter J. Peroral administration of nanoparticles. *Adv Drug Deliv Rev*. 1991;7:71–86.
12. Kreuter J. Nanoparticle-based drug delivery systems. *J Control Release*. 1991;16:169–176.
13. Kreuter J. Nanoparticles. In: Swarbrick J, Boylan JC. editors. *Encyclopedia of Pharmaceutical Technology*. New York: Marcel Dekker, 1994:165–190.
14. Brannon-Peppas L, Blanchette JO. Nanoparticle and targeted systems for cancer therapy. *Adv Drug Deliv Rev*. 2004;56:1649–1659.
15. Brannon-Peppas L. Recent advances on the use of biodegradable microparticles and nanoparticles in controlled drug delivery. *Int J Pharm*. 1995;116:1–9.
16. Hamoudeh M, Fessi H. Preparation, characterization and surface study of poly-epsilon caprolactone magnetic microparticles. *J Colloid Interface Sci*. 2006;300:584–590.
17. Guinebretière S, Briançon S, Fessi H, Teodorescu VS, Blanchin MG. Nanocapsules of biodegradable polymers: preparation and characterization by direct high resolution electron microscopy. *Mater Sci Eng C*. 2002;21:137–142.
18. Yu W, Tabosa do Egito ES, Barratt G, Fessi H, Devissaguet JP, Puisieux F. A novel approach to the preparation of injectable emulsions by a spontaneous emulsification process. *Int J Pharm*. 1993;89:139–146.
19. Fessi H, Puisieux F, Devissaguet JP, Ammoury N, Benita S. Nanocapsule formation by interfacial polymer deposition following solvent displacement. *Int J Pharm*. 1989;55:R1–R4.
20. Naumann EB, Qiwei He D. Nonlinear diffusion and phase separation. *Chem Eng Sci*. 2001;56:1999–2018.
21. Flory PJ. Thermodynamics of high polymer solutions. *J Chem Phys*. 1942;10:51–61.
22. Quintanar-Guerrero D, Allémann E, Fessi H, Doelker E. Pseudolatex preparation using a novel emulsion–diffusion process involving direct displacement of partially water-miscible solvents by distillation. *Int J Pharm*. 1999;188:155–164.
23. Danilatos GD, Postle R. The environmental scanning electron microscope and its applications. *Scanning Electron Microscope*. 1982;1:1–16.
24. Krishna R, Wesselingh JA. The Maxwell-Stefan approach to mass transfer. *Chem Eng Sci*. 1997;52:861–911.
25. Hoch G, Chauhan A, Radke CJJ. Permeability and diffusivity for water transport through hydrogel membranes. *Membr Sci*. 2003;214:199–209.
26. Bausa J, Marquardt W. Detailed modeling of stationary and transient mass transfer across pervaporation membranes. *AIChE J*. 2001;47:1318–1332.
27. Paul DR. Reformulation of the solution–diffusion theory of reverse osmosis. *J Membr Sci*. 2004;241:371–386.
28. Schaetzel P, Bendjama Z, Vauclair C, Nguyen QT. The solution–diffusion model—order of magnitude calculation of coupling between the fluxes in pervaporation. *J Membr Sci*. 2001;191:95–102.
29. Schaetzel P, Favre E, Auclair B, Nguyen QT. Mass-transfer through ion exchange membranes: comparison between the diffusion and the diffusion-convection Stefan-Maxwell equations. *Electrochim Acta*. 1997;42:2475–2483.
30. Zielinski JM, Hanley BF. Practical friction-based approach to modeling multicomponent diffusion. *AIChE J*. 1999;45:1–12.
31. Meyers JP, Newman J. Simulation of the direct methanol fuel cell I. Thermodynamic framework for a multi-component membrane. *J Electrochem Soc*. 2002;149:A718–A728.
32. Fornasiero F, Prausnitz JM, Radke CJ. Multicomponent diffusion in highly asymmetric systems. An extended Maxwell-Stefan model for Starkly different-sized segment-accessible chain molecules. *Macromolecules*. 2005;38:1364–1370.
33. Flory P. *Principles of Polymer Chemistry*. Ithaca, New York: Cornell University Press, 1953.
34. Vrentas JS, Vrentas CM. Drying of solvent coated polymer films. *J Polym Sci Part B: Polym Phys*. 1994;32:187.
35. Bouchemal K, Couenne F, Briançon S, Fessi H, Tayakout M. Polyamides nanocapsules: modeling and wall thickness estimation. *AIChE J*. 2006;52:2161–2170.
36. Wakao N, Funazkri T. Effect of fluid dispersion coefficients on particle-to-fluid mass transfer coefficients in packed beds. Correlation of Sherwood numbers. *Chem Eng Sci*. 1978;33:1375–1384.
37. Vignes A. Diffusion in binary solutions. *Ind Eng Chem Fundam*. 1966;5:189–199.
38. Wilke CR, Chang P. Correlation of diffusion coefficient in dilute solutions. *AIChE J*. 2004;1:264–270.
39. Guinebretière S, Briançon S, Lieto J, Mayer C, Fessi H. Study of the emulsion–diffusion of solvent: Preparation and characterization of nanocapsules, *Drug Dev Res*. 2002;57:18–33.
40. Loxley A, Vincent B. Preparation of poly(methylmethacrylate) microcapsules with liquid cores. *J Colloid Interface Sci*. 1998;208:49–62.

Appendix

Spatial discretization

The spatial domain is initially discretized using a one-dimensional spherical grid (with a positive orientation from center to exterior of the sphere). To write the scheme of discretization in J, we indicate the node by $J + 1$ and $J - 1$ located immediately on its right and its left (Figure A1). The "control volume" is centered in J and has a Δr length.

We assume that the flux leaving one control volume is the same as the one entering in the adjacent volume. Inside each volume, both physical and chemical properties are considered to be constant and equal to the volume-average value.

$\bar{x}$ is defined as the volume-average value of the variable x in the volume V. It is given by the following equation:

$$\bar{x} \equiv \frac{1}{V}\int_V x dV \tag{A1}$$

Equivalently in spherical coordinates

$$\bar{x} \equiv \frac{3}{R^3}\int_0^R x r^2 dr \tag{A2}$$

Since the number of finite volumes is fixed, the boundary coordinates of each volume are variable (because of the moving interface). As a consequence, we use the Leibniz integral rule to calculate the integral of the continuity equation.

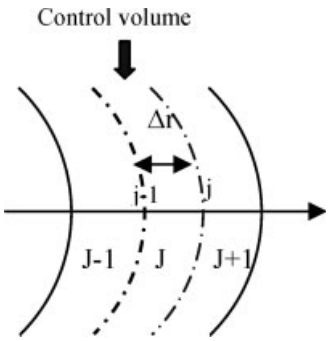

Figure A1. Scheme of discretization.

To facilitate the numerical treatment of the moving interface, the following coordinate transformation is used:

$$\xi = \frac{r}{R_t} \quad \text{for } 0 \le r \le R_t \quad \text{and} \quad 0 \le \xi \le 1 \tag{A3}$$

Accordingly

$$\xi(r,t) = \frac{r}{R_t} \quad \text{for } 0 \le r \le R_t \tag{A4}$$

With such change of coordinate, the boundary of the domain remains fixed: $0 \le \xi \le 1$.

The continuity equation for each component in each volume becomes:

$$\begin{aligned} &\frac{d}{dt}\int_{r_{j-1}}^{r_j} \frac{4\pi}{3}\phi_i(t,r)r^2 dr \\ &= \int_{r_{j-1}}^{r_j} \frac{d\phi_i(t,r)}{dt} 4\pi r^2 dr + 4\pi r_{j+1}^2 \phi(t,r_{j+1})\frac{dr_{j+1}}{dt} \\ &- 4\pi r_j^2 \phi_i(t,r_j)\frac{dr_j}{dt} \\ &= -v_i^0 \int_{r_{j-1}}^{r_j} 4\pi \frac{\partial(r^2 N_i^0(r))}{\partial r} dr \end{aligned} \tag{A5}$$

Replacing $\frac{dr_j}{dt}$ and $\frac{dr_{j+1}}{dt}$ by their values, Eq. A4 becomes

$$\begin{aligned} &\frac{1}{3}\left(\xi_j^3 - \xi_{j-1}^3\right)\left.\overline{\frac{\partial\phi_i}{\partial t}}\right|_j - \frac{1}{R(t)}\frac{\partial R_t}{\partial t}\left[\left(\left.\xi_j^3(\overline{\phi_i})\right|_{j+1} - \left.\xi_{j-1}^3(\overline{\phi_i})\right|_j\right)\right. \\ &\left. -\left(\xi_j^3 - \xi_{j-1}^3\right)\left(\left.\overline{\phi_i}\right|_j\right)\right] = -\frac{v_i^0}{R(t)}\left[\left.\left(\xi^2 N_i^0\right)\right|_j - \left.\left(\xi^2 N_i^0\right)\right|_{j-1}\right] \end{aligned} \tag{A6}$$

The development of the continuity equation in the case of moving boundaries appear as a convection term relative to the solvent diffusion inside the nanocapsule. This term is due to the fact that the solvent diffusion is compensated by the volume reduction.

Then the boundary conditions are expressed by:

$$\text{At } \xi = 1 \qquad \frac{\left(N_i^0\right)\big|_{\xi=1}}{n_s^i} - \frac{dR_t}{dt}\frac{\phi_i|_{\xi=1}}{n_s^i v_i^0} = 0 \quad i = 2,3 \tag{A7}$$

$$\frac{\left(N_1^0\right)\big|_{\xi=1}}{n_s^1} - \frac{dR_t}{dt}\frac{\phi_1|_{\xi=1}}{n_s^1 v_i^0} = K_1(c_1^* - c_1^{\text{ext}}) \tag{A8}$$

Manuscript received Apr. 30, 2008, revision received Oct. 17, 2008, and final revision received Dec. 12, 2008.